


Article

Unusual Spin Exchanges Mediated by the Molecular Anion $P_2S_6^{4-}$: Theoretical Analyses of the Magnetic Ground States, Magnetic Anisotropy and Spin Exchanges of MPS_3 (M = Mn, Fe, Co, Ni)

Hyun-Joo Koo ^{1,*}, Reinhard Kremer ² and Myung-Hwan Whangbo ^{1,3,*} ¹ Department of Chemistry and Research Institute for Basic Sciences, Kyung Hee University, Seoul 02447, Korea² Max Planck Institute for Solid State Research, Heisenbergstrasse 1, D-70569 Stuttgart, Germany; rekre@mpg.fkf.de³ Department of Chemistry, North Carolina State University, Raleigh, NC 27695-8204, USA

* Correspondence: hjkoo@khu.ac.kr (H.-J.K.); mike_whangbo@ncsu.edu (M.-H.W.)

Abstract: We examined the magnetic ground states, the preferred spin orientations and the spin exchanges of four layered phases MPS_3 (M = Mn, Fe, Co, Ni) by first principles density functional theory plus onsite repulsion (DFT + U) calculations. The magnetic ground states predicted for MPS_3 by DFT + U calculations using their optimized crystal structures are in agreement with experiment for M = Mn, Co and Ni, but not for Fe PS_3 . DFT + U calculations including spin-orbit coupling correctly predict the observed spin orientations for Fe PS_3 , Co PS_3 and Ni PS_3 , but not for Mn PS_3 . Further analyses suggest that the $|l_z|$ spin direction observed for the Mn^{2+} ions of Mn PS_3 is caused by the magnetic dipole–dipole interaction in its magnetic ground state. Noting that the spin exchanges are determined by the ligand p-orbital tails of magnetic orbitals, we formulated qualitative rules governing spin exchanges as the guidelines for discussing and estimating the spin exchanges of magnetic solids. Use of these rules allowed us to recognize several unusual exchanges of MPS_3 , which are mediated by the symmetry-adapted group orbitals of $P_2S_6^{4-}$ and exhibit unusual features unknown from other types of spin exchanges.

Keywords: magnetic ground state; spin exchange; magnetic anisotropy; molecular anion; MPS_3 ; magnetic orbitals; qualitative rules



Citation: Koo, H.-J.; Kremer, R.; Whangbo, M.-H. Unusual Spin Exchanges Mediated by the Molecular Anion $P_2S_6^{4-}$: Theoretical Analyses of the Magnetic Ground States, Magnetic Anisotropy and Spin Exchanges of MPS_3 (M = Mn, Fe, Co, Ni). *Molecules* **2021**, *26*, 1410.

<https://doi.org/10.3390/molecules26051410>

molecules26051410

Academic Editor: Takashiro Akitsu

Received: 27 January 2021

Accepted: 26 February 2021

Published: 5 March 2021

Publisher's Note: MDPI stays neutral with regard to jurisdictional claims in published maps and institutional affiliations.



Copyright: © 2021 by the authors. Licensee MDPI, Basel, Switzerland. This article is an open access article distributed under the terms and conditions of the Creative Commons Attribution (CC BY) license (<https://creativecommons.org/licenses/by/4.0/>).

1. Introduction

In an extended solid, transition-metal magnetic cations M are surrounded by main-group ligands L to form ML_n (typically, $n = 3–6$) polyhedra, and the unpaired spins of M are accommodated in the singly occupied d-states (i.e., the magnetic orbitals) of ML_n . Each d-state has the metal d-orbital combined out-of-phase with the p-orbitals of the surrounding ligands L. The tendency for two adjacent magnetic ions to have a ferromagnetic (FM) or an antiferromagnetic (AFM) spin alignment is determined by the spin exchange between them, which takes place through the M-L-M or M-L ... L-M exchange path [1–4]. Whereas the characteristics (e.g., the angular and distance dependence) of the M-L-M exchanges is conceptually well understood [5–8], the properties of the M-L ... L-M exchanges involving several main-group ligands have only come into focus in the last two decades [1–4]. Furthermore, the character of a M-L ... L-M exchange can be modified if the L ... L contact is bridged by a d^0 metal cation A to form a L ... A ... L bridge [1–4]. What has not been well understood so far is the M-L ... L-M exchange in which the L ... L contact is an integral part of the covalent framework of a molecular anion made up of main group elements (e.g., the $P_2S_6^{4-}$ anion in MPS_3 , where M = Mn, Fe, Co, Ni), which might be termed the M-(L-L)-M exchange to emphasize its difference from the M-L-M, M-L ... L-M and M-L ... A ... L-M exchanges.

In the present work we examine the M-(L-L)-M spin exchanges in the layered phases MPS_3 ($M = \text{Mn}$ [9–11], Fe [9–11], Co [10,11], Ni [10,11]), which crystallize with a monoclinic structure (space group $C2/m$, no. 12). Each layer of MPS_3 is made up of the molecular anions $\text{P}_2\text{S}_6^{4-}$ possessing the structure of staggered ethane (i.e., a trigonal antiprism structure) (Figure 1a,b). The molecular anions $\text{P}_2\text{S}_6^{4-}$ form a trigonal layer (Figure 1c) with the P-P bonds perpendicular to the layer, and a high-spin M^{2+} cation occupies every S_6 octahedral site (deviations from a trigonal symmetry caused by the monoclinic distortions are less than 1°). Thus, each MPS_3 layer consists of a honeycomb arrangement of M^{2+} cations. With the c^* -direction of the MPS_3 taken as the z -direction, the P-P bond of each $\text{P}_2\text{S}_6^{4-}$ is parallel to the z -direction ($\parallel z$), and each MS_6 octahedron is arranged with one of its three-fold rotational axes along the $\parallel z$ -direction.

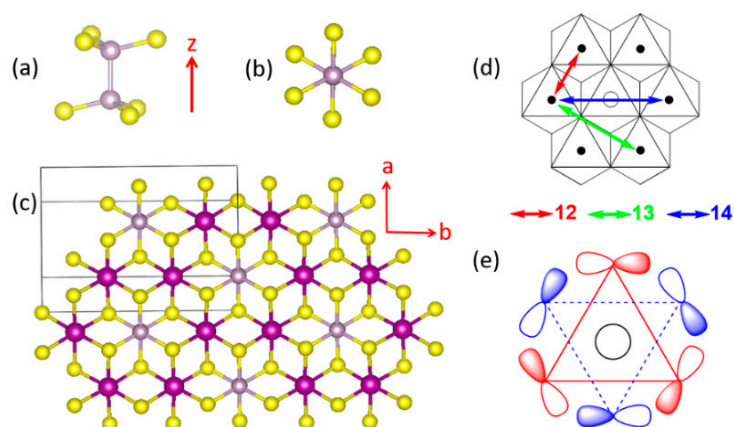


Figure 1. (a) Perspective and (b) projection views of a $\text{P}_2\text{S}_6^{4-}$ anion. (c) A projection view of a single MPS_3 layer along the c^* -direction (i.e., the z -direction), which is perpendicular to the MPS_3 layer. (d) Three kinds of the spin exchange paths in the MPS_3 honeycomb layers of MPS_3 , where the labels 12, 13 and 14 refer to J_{12} , J_{13} and J_{14} , respectively. (e) A group orbital of $\text{P}_2\text{S}_6^{4-}$ viewed along the P-P axis. The red triangle represents the three S atoms of the upper PS_3 pyramid, and the blue triangles those of the lower PS_3 pyramid.

To a first approximation, it may be assumed that each MPS_3 layer has a trigonal symmetry (see below for further discussion), so there are three types of spin exchanges to consider, i.e., the first nearest-neighbor (NN) spin exchange J_{12} , the second NN spin exchange J_{13} , and the third NN exchange J_{14} (Figure 1d). J_{12} is a spin exchange of the M-L-M type, in which the two metal ions share a common ligand, while J_{13} and J_{14} are nominally spin exchanges of the M-L . . . L-M type, in which the two metal ions do not share a common ligand. In describing the magnetic properties of MPS_3 in terms of the spin exchanges J_{12} , J_{13} and J_{14} , an interesting conceptual problem arises. Each $\text{P}_2\text{S}_6^{4-}$ anion is coordinated to the six surrounding M^{2+} cations simultaneously (Figure 1c,d), so one $\text{P}_2\text{S}_6^{4-}$ anion participates in all three different types of spin exchanges simultaneously with the surrounding six M^{2+} ions. Furthermore, the lone-pair orbitals of the S atoms of $\text{P}_2\text{S}_6^{4-}$, responsible for the coordination with M^{2+} ions, form symmetry-adapted group orbitals, in which all six S atoms participate (for example, see Figure 1e). Consequently, there is no qualitative argument with which to even guess the possible differences in J_{12} , J_{13} , and J_{14} . Over the past two decades, it became almost routine to quantitatively determine any spin exchanges of a magnetic solid by performing an energy-mapping analysis based on first principles DFT calculations. From a conceptual point of view, it would be very useful to have qualitative rules with which to judge whether the spin exchange paths involving complex intermediates are usual or unusual.

A number of experimental studies examined the magnetic properties of MPS_3 ($M = \text{Mn}$ [9,11–14], Fe [9,11,15–18], Co [11,19], Ni [11,20]). The magnetic properties of MPS_3 ($M = \text{Mn}$, Fe , Co , Ni) monolayers were examined by DFT calculations to find their potential use as single-layer materials

possessing magnetic order [21]. The present work is focused on the magnetic properties of bulk MPS_3 . For the ordered AFM states of MPS_3 , the neutron diffraction studies reported that the layers of $MnPS_3$ exhibits a honeycomb-type AFM spin arrangement, AF1 (Figure 2a), but those of $FePS_3$, $CoPS_3$ and $NiPS_3$ a zigzag-chain spin array, AF2 (Figure 2b), in which the FM chains running along the a -direction are antiferromagnetically coupled (hereafter, the $\parallel a$ -chain arrangement). An alternative AFM arrangement, AF3 (Figure 2c), in which the FM zigzag chains running along the $(a+b)$ -direction are antiferromagnetically coupled (hereafter, the $\parallel(a+b)$ -chain arrangement), is quite similar in nature to the $\parallel a$ -chain arrangement.

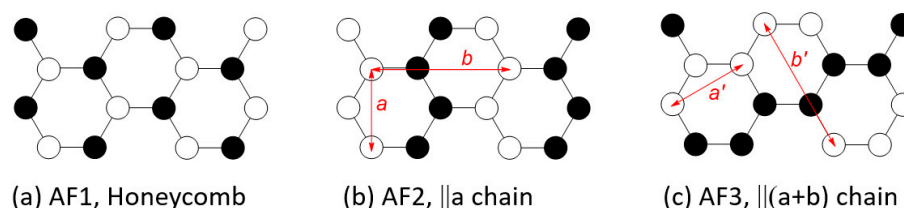


Figure 2. (a) The honeycomb AFM state, AF1. (b) The $\parallel a$ -chain AFM state, AF2. (c) The $\parallel(a+b)$ -chain AFM state, AF3.

At present, it is unclear why the spin arrangement of $MnPS_3$ differs from those of $FePS_3$, $CoPS_3$ and $NiPS_3$ and why $FePS_3$, $CoPS_3$ and $NiPS_3$ all adopt the $\parallel a$ -chain arrangement rather than the $\parallel(a+b)$ -chain arrangement. To explore these questions, it is necessary to examine the relative stabilities of a number of possible ordered spin arrangements of MPS_3 ($M = Mn, Fe, Co, Ni$) by electronic structure calculations and analyze the spin exchanges of their spin lattices.

Other quantities of importance for the magnetic ions M of an extended solid are the preferred orientations of their magnetic moments with respect to the local coordinates of the ML_n polyhedra. These quantities, i.e., the magnetic anisotropy energies, are also readily determined by DFT calculations including spin orbit coupling (SOC). For the purpose of interpreting the results of these calculations, the selection rules for the preferred spin orientation of ML_n were formulated [2,3,22–24] based on the SOC-induced interactions between the highest-occupied molecular orbital (HOMO) and lowest-unoccupied molecular orbital (LUMO) of ML_n . With the local z -axis of ML_n taken along its n -fold rotational axis ($n = 3, 4$), the quantity needed for the selection rules is the minimum difference, $|\Delta L_z|$, in the magnetic quantum numbers L_z of the d -states describing the angular behaviors of the HOMO and LUMO. It is of interest to analyze the preferred spin orientations of the M^{2+} ions in MPS_3 ($M = Mn, Fe, Co, Ni$) from the viewpoint of the selection rules.

Our work is organized as follows: Section 2 describes simple qualitative rules governing spin exchanges. The details of our DFT calculations are presented in Section 3.1. The magnetic ground states of MPS_3 ($M = Mn, Fe, Co, Ni$) are discussed in Section 3.2, the preferred spin orientations of M^{2+} ions of MPS_3 in Section 3.3, and the quantitative values of the spin exchanges determined for MPS_3 in Section 3.4. We analyze the unusual features of the calculated spin exchanges via the $P_2S_6^{4-}$ anion in Section 3.5, and investigate in Section 3.6 the consequences of the simplifying assumption that the honeycomb spin lattice has a trigonal symmetry rather than a slight monoclinic distortion found experimentally. Our concluding remarks are summarized in Section 4.

2. Qualitative Rules Governing Spin Exchanges

2.1. Spin Exchange between Magnetic Orbitals

For clarity, we use the notation (φ_i, φ_j) to represent the spin exchange arising from the magnetic orbitals φ_i and φ_j at the magnetic ion sites A and B , respectively. It is well known that (φ_i, φ_j) consists of two competing terms [1–4,25]

$$(\varphi_i, \varphi_j) = J_F + J_{AF} \quad (1)$$

The FM component J_F (>0) is proportional to the exchange repulsion,

$$J_F \propto K_{ij} \quad (2)$$

which increases with increasing the overlap electron density $\rho_{ij} = \varphi_i \varphi_j$. In case when the magnetic orbitals φ_i and φ_j are degenerate (e.g., between the t_{2g} states or between e_g states of the magnetic ions at octahedral sites), the AFM component J_{AF} (<0) is proportional to the square of the energy split Δe_{ij} between φ_i and φ_j induced by the interaction between them,

$$J_{AF} \propto -(\Delta e_{ij})^2 \propto -(S_{ij})^2 \quad (3)$$

The energy split Δe_{ij} is proportional to the overlap integral $S_{ij} = \langle \varphi_i | \varphi_j \rangle$, so that the magnitude of the AFM component J_{AF} increases with increasing that of $(S_{ij})^2$. If φ_i and φ_j are not degenerate (e.g., between the t_{2g} and e_g states of the magnetic ions), the magnitude of J_{AF} is approximately proportional to $-(S_{ij})^2$.

2.2. p-Orbital Tails of Magnetic Orbitals

The spin exchanges between adjacent transition-metal cations M are determined by the interactions between their magnetic orbitals, which in turn are governed largely by the overlap and the overlap electron density that are generated by the p-orbitals of the ligands present in the magnetic orbitals (the p-orbital tails, for short) [1–4]. Suppose that the metal ions M are surrounded by main-group ligands L to form ML_6 octahedra. In the t_{2g} and e_g states of an ML_6 octahedron (Figure 3a,b), the d-orbitals of M make σ and π antibonding combinations with the p-orbitals of the ligands L. Thus, the p-orbital tails of the t_{2g} and e_g states are represented as in Figure 4a,b, respectively, so that each M-L bond has the p_π and p_σ tails in the t_{2g} and e_g states, respectively, as depicted in Figure 4c. The triple-degeneracy of the t_{2g} and the double-degeneracy of the e_g states are lifted in a ML_5 square pyramid and a ML_4 square plane, both of which have a four-fold rotational symmetry; the t_{2g} states (xz, yz, xy) are split into (xz, yz) and xy , and the e_g states ($3z^2 - r^2, x^2 - y^2$) into $3z^2 - r^2$ and $x^2 - y^2$. Nevertheless, the description of the ligand p-orbital tails of the d-states depicted in Figure 4c remains valid.

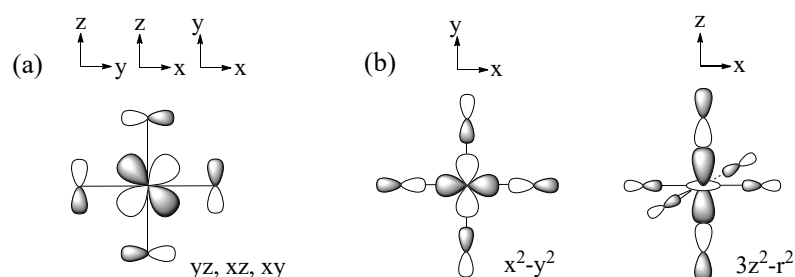


Figure 3. (a) The t_{2g} states and (b) the e_g states of a ML_6 octahedron.

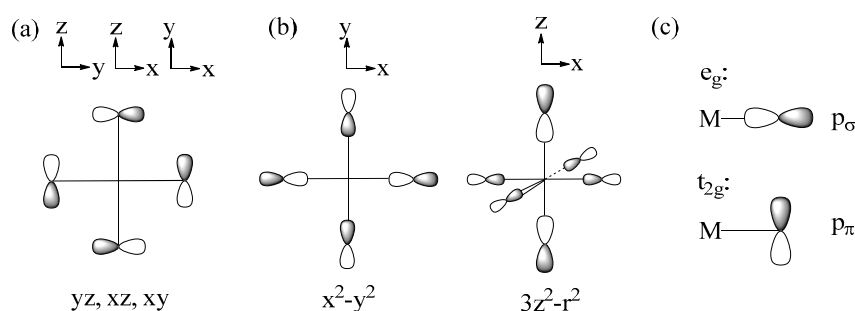


Figure 4. The p-orbital tails of (a) the t_{2g} and (b) the e_g states of a ML_6 octahedron. (c) The p_σ and p_π orbitals of the ligand p-orbital tails.

2.3. Spin Exchanges in Terms of the *p*-Orbital Tails

In this section, we generalize the qualitative rules of spin exchanges formulated for the magnetic solids of Cu^{2+} ions [4]. Each Cu^{2+} ion has only one magnetic orbital, i.e., the x^2-y^2 state in which each Cu-L bond has a p_σ tail. The d-electron configuration of the magnetic ion is $(t_{2g}\uparrow)^3(e_g\uparrow)^2(t_{2g}\downarrow)^0(e_g\downarrow)^0$ in MnPS_3 , $(t_{2g}\uparrow)^3(e_g\uparrow)^2(t_{2g}\downarrow)^1(e_g\downarrow)^0$ in FePS_3 , $(t_{2g}\uparrow)^3(e_g\uparrow)^2(t_{2g}\downarrow)^2(e_g\downarrow)^0$ in CoPS_3 , and $(t_{2g}\uparrow)^3(e_g\uparrow)^2(t_{2g}\downarrow)^3(e_g\downarrow)^0$ in NiPS_3 . Thus, the Mn^{2+} , Fe^{2+} , Co^{2+} , and Ni^{2+} ions possess 5, 4, 3, and 2 magnetic orbitals, respectively. For magnetic ions with several magnetic orbitals, the spin exchange J_{AB} between two such ions located at sites A and B is given by the sum of all possible individual exchanges (φ_i, φ_j) ,

$$J_{AB} = \frac{2}{n_A n_B} \sum_{i \in A} \sum_{j \in B} (\varphi_i, \varphi_j) \propto \sum_{i \in A} \sum_{j \in B} (\varphi_i, \varphi_j) \quad (4)$$

where n_A and n_B are the number of magnetic orbitals at the sites A and B, respectively. Each individual exchange (φ_i, φ_j) can be FM or AFM depending on which term, J_F or J_{AF} , dominates. Whether J_{AB} is FM or AFM depends on the sum of all individual (φ_i, φ_j) contributions.

2.3.1. M-L-M Exchange

As shown in Figure 5, there occur three types of M-L-M exchanges between the magnetic orbitals of t_{2g} and e_g states.

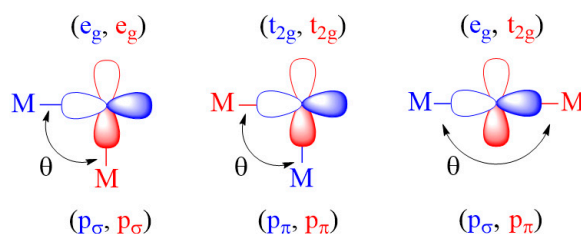


Figure 5. Three-types of M-L-M spin exchanges between t_{2g} and e_g magnetic orbitals.

If the M-L-M bond angle θ is 90° for the (e_g, e_g) and (t_{2g}, t_{2g}) exchanges, and also when θ is 180° for the (e_g, t_{2g}) exchange, the two *p*-orbital tails have an orthogonal arrangement so that $\langle \varphi_i | \varphi_j \rangle = 0$ (i.e., $J_{AF} = 0$). However, the overlap electron density $\varphi_i \varphi_j$ is nonzero (i.e., $J_F \neq 0$), hence predicting these spin exchanges to be FM. When the θ angles of the (e_g, e_g) and (t_{2g}, t_{2g}) exchanges increase from 90° toward 180° , and also when the angle θ of the (e_g, t_{2g}) exchange decreases from 180° toward 90° , both J_{AF} and J_F are nonzero so that the balance between the two determines if the overall exchange (φ_i, φ_j) becomes FM or AFM. These trends are what the Goodenough–Kanamori rules [5–8] predict.

2.3.2. M-L ... L-M Exchange

There are two extreme cases of M-L ... L-M exchange. When the p_σ -orbital tails are pointing toward each other (Figure 6a), the overlap integral, $\langle \varphi_i | \varphi_j \rangle$, can be substantial if the contact distance L ... L lies in the vicinity of the van der Waals distance. However, the overlap electron density $\rho_{ij} = \varphi_i \varphi_j$ is practically zero because φ_i and φ_j do not have an overlapping region. Consequently, the in-phase and out-of-phase states Ψ_+ and Ψ_- are split in energy with a large separation Δe_{ij} . Thus, it is predicted that the M-L ... L-M type exchange can only be AFM [1–4]. When the L ... L linkage is bridged by a d^0 cation such as V^{5+} or W^{6+} , for example, only the out-of-phase state Ψ_- is lowered in energy by the d_π orbital of the cation A, reducing the Δe_{ij} so that the M-L ... A ... L-M exchange becomes weak (Figure 6b). Conversely, when the *p*-orbital tails of the M-L ... L-M exchange path have an orthogonal arrangement (Figure 7a), the overlap integral, $\langle \varphi_i | \varphi_j \rangle$, is zero, making the M-L ... L-M exchange weak. If the L ... L linkage of such an exchange path is bridged

by a d^0 cation, the out-of-phase state Ψ_- level is lowered in energy enlarging Δe_{ij} so that the M-L ... A ... L-M becomes strongly AFM (Figure 7b) [2–4].

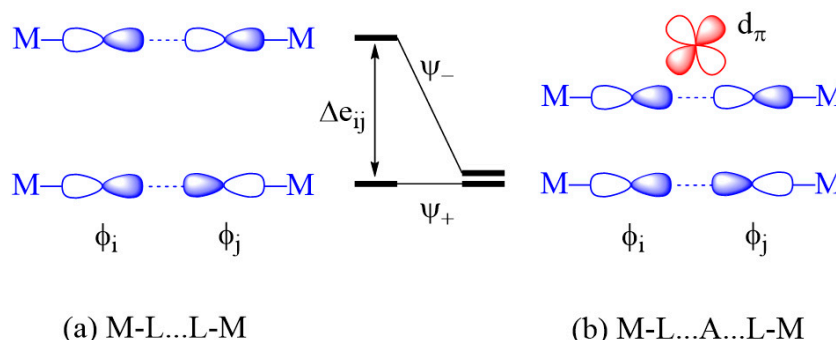


Figure 6. Interactions between the magnetic orbitals in the M-L ... L-M exchange where their p_σ tails are pointing to each other. The large energy split Δe_{ij} of the M-L ... L-M exchange in (a) is reduced by the d_π orbital of the d^0 cation A in the M-L ... A ... L-M exchange in (b).

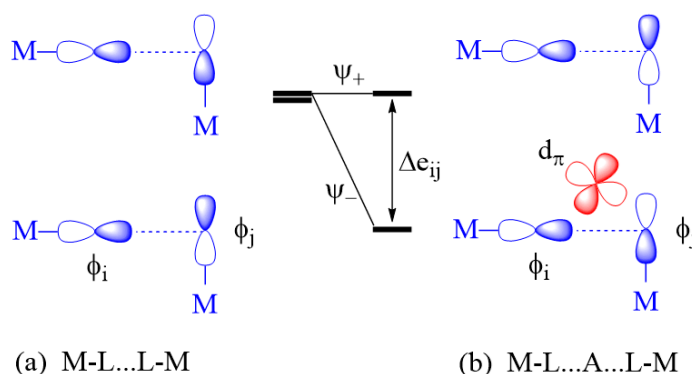


Figure 7. Interactions between the magnetic orbitals in the M-L ... L-M exchange where their p_σ tails have an orthogonal arrangement. The small energy split Δe_{ij} of the M-L ... L-M exchange in (a) is enlarged by the d_π orbital of the d^0 cation A in the M-L ... A ... L-M exchange in (b).

In the M-L ... A ... L-M exchange of Figure 7, the vanishingly small Δe_{ij} of the M-L ... L-M exchange results because the two p_σ tails have an orthogonal arrangement. A very small Δe_{ij} for the M-L ... L-M exchange occurs even if the two M-L bonds are pointing to each other as in Figure 6 when one M-L bond has a p_σ tail and the other has a p_π tail, and also when both M-L bonds have p_π tails. Such M-L ... L-M spin exchanges become strong in the corresponding M-L ... A ... L-M exchanges.

2.3.3. Qualitative Rules Governing Spin Exchanges

The above discussions are based on the observation that the nature of a spin exchange, be it the M-L-M, M-L ... L-M or M-L ... A ... L-M type, is governed by the ligand p-orbital tails present in the magnetic orbitals of the spin exchange path. The essential points of our discussions can be summarized as follows:

- a. For an individual (φ_i, φ_j) exchange of a M-L-M type, the (t_{2g}, t_{2g}) and (e_g, e_g) exchanges are FM if the bond angle θ is 90° , and so is the (t_{2g}, e_g) exchange if the bond angle θ is 180° . These exchanges become AFM when the bond angles θ deviate considerably from these values.
- b. An individual (φ_i, φ_j) exchange of a M-L ... L-M or M-L ... A ... L-M type can only be AFM if not weak.
- c. A strong individual (φ_i, φ_j) exchange of a M-L ... L-M is weakened by the d^0 metal cation A in the M-L ... A ... L-M exchange, but a weak individual (φ_i, φ_j) exchange

of a M-L ... L-M is strengthened by the presence of a d^0 metal cation A in the M-L ... A ... L-M exchange.

- d. When a magnetic ion has several unpaired spins, the spin exchange between two magnetic ions is given by the sum of all possible individual (φ_i, φ_j) exchanges.

These qualitative rules governing spin exchanges can serve as guidelines for exploring how the calculated spin exchanges are related to the structures of the exchange paths and also for ensuring that important exchange paths are included the set of spin exchanges to evaluate by the energy-mapping analysis.

3. Results and Discussion

3.1. Details of Calculations

We performed spin-polarized DFT calculations using the Vienna ab initio Simulation Package (VASP) [26,27], the projector augmented wave (PAW) method, and the PBE exchange-correlation functionals [28]. The electron correlation associated with the 3d states of M (M = Mn, Fe, Co, Ni) was taken into consideration by performing the DFT+U calculations [29] with the effective on-site repulsion $U_{\text{eff}} = U - J = 4$ eV on the magnetic ions. Our DFT + U calculations carried out for numerous magnetic solids of transition-metal ions showed that use of the U_{eff} values in the range of 3 – 5 eV correctly reproduce their magnetic properties (see the original papers cited in the review articles [1–3,22,24]). The primary purpose of using DFT + U calculations is to produce magnetic insulating states for magnetic solids. Use of $U_{\text{eff}} = 3 - 5$ eV in DFT + U calculations leads to magnetic insulating states for magnetic solids of Mn^{2+} , Fe^{2+} , Co^{2+} , and Ni^{2+} ions. The present work employed the representative U_{eff} value of 4 eV. We carried out DFT + U calculations (with $U_{\text{eff}} = 4$ eV) to optimize the structures of MPS_3 (M = Mn, Fe, Co, Ni) in their FM states by relaxing only the ion positions while keeping the cell parameters fixed and using a set of $(4 \times 2 \times 6)$ k-points and the criterion of 5×10^{-3} eV/Å for the ionic relaxation. All our DFT + U calculations for extracting the spin-exchange parameters employed a $(2a, 2b, c)$ supercell, the plane wave cutoff energy of 450 eV, the threshold of 10^{-6} eV for self-consistent-field energy convergence, and a set of $(4 \times 2 \times 6)$ k-points. The preferred spin direction of the cation M^{2+} (M = Mn, Fe, Co, Ni) cation was determined by DFT + U + SOC calculations [30], employing a set of $(4 \times 2 \times 6)$ k-points and the threshold of 10^{-6} eV for self-consistent-field energy convergence.

3.2. Magnetic Ground States of MPS_3

We probed the magnetic ground states of the MPS_3 phases by evaluating the relative energies, on the basis of DFT + U calculations, of the AF1, AF2 and AF3 spin configurations shown in Figure 2 as well as the FM, AF4, AF5, and AF6 states depicted in Supplementary Materials, Figure S1. As summarized in Table 1, our calculations using the experimental structures of MPS_3 show that the magnetic ground states of MnPS_3 and NiPS_3 adopt the honeycomb state AF1 and the $||a$ -chain state AF2, respectively, in agreement with experiment. In disagreement with experiment, however, the magnetic ground state is predicted to be the $|| (a+b)$ -chain state AF3 for FePS_3 , and the honeycomb state AF1 for CoPS_3 . Since the energy differences between different spin ordered states are small, it is reasonable to speculate if they may be affected by small structural (monoclinic) distortion. Thus, we optimize the crystal structures of MPS_3 (M = Mn, Fe, Co, Ni) by performing DFT + U calculations to obtain the structures presented in the supporting material. Then, we redetermined the relative stabilities of the FM and AF1–AF6 states using these optimized structures. Results of these calculations are also summarized in Table 1. The optimized structures predict that the magnetic ground states of MnPS_3 , CoPS_3 and NiPS_3 are the same as those observed experimentally, but that of FePS_3 is still the $|| (a+b)$ -chain state AF3 rather than the $||a$ -chain state AF2 reported experimentally. This result is not a consequence of using the specific value of $U_{\text{eff}} = 4$ eV, because our DFT + U calculations for FePS_3 with $U_{\text{eff}} = 3.5$ and 4.5 eV lead to the same conclusion.

Table 1. Relative energies (in meV/formula unit) obtained for the seven ordered spin states of MPS_3 ($M = Mn, Fe, Co, Ni$) from DFT + U calculations with $U_{eff} = 4$ eV. The numbers without parentheses are obtained by using the experimental structures, and those in parentheses by using the structures optimized by DFT + U calculations.

	Mn	Fe	Co	Ni
FM	33.77 (33.36)	31.25 (25.10)	71.46 (55.00)	45.00 (42.04)
AF1	0 (0)	12.24 (5.16)	0 (5.70)	6.50 (7.11)
AF2	15.54 (15.50)	12.92 (7.93)	45.05 (0)	0 (0)
AF3	14.25 (14.21)	0 (0)	34.02 (24.99)	0.35 (0.34)
AF4	14.72 (14.45)	20.85 (18.57)	22.16 (26.00)	52.40 (49.53)
AF5	12.77 (12.58)	15.79 (12.95)	157.25 (158.33)	33.62 (31.98)
AF6	17.24 (17.07)	10.57 (6.33)	140.58 (143.05)	16.43 (15.21)

To resolve the discrepancy between theory and experiment on the magnetic ground state of $FePS_3$, we note that the magnetic peak positions in the neutron diffraction profiles are determined by the repeat distances of the rectangular magnetic structures, namely, a and b for the AF2 state (Figure 2b), and a' and b' for the AF3 state (Figure 2c). In both the experimental and the optimized structures of $FePS_3$, it was found that $a = a' = 5.947$ Å and $b = b' = 10.300$ Å. Thus, for the neutron diffraction refinement of the magnetic structure for $FePS_3$, the AF2 and AF3 states provide an equally good model. In view of our computational results, we conclude that the AF3 state is the correct magnetic ground state for $FePS_3$.

The experimental and optimized structures of MPS_3 ($M = Mn, Fe, Co, Ni$) are very similar, as expected. The important differences between them affecting the magnetic ground state would be the M-S distances of the MS_6 octahedra, because the d-state splitting of the MS_6 octahedra is sensitively affected by them. The M-S distances of the MS_6 octahedra taken from the experimental and optimized crystal structures of MPS_3 are summarized in Table 2, and their arrangements in the honeycomb layer are schematically presented in Figure 8. All Mn-S bonds of MnS_6 in $MnPS_3$ are nearly equal in length, as expected for a high-spin d^5 ion (Mn^{2+}) environment. The Fe-S bonds of FeS_6 in the optimized structure of $FePS_3$ are grouped into two short and four long Fe-S bonds. This distinction is less clear in the experimental structure. The Co-S bonds of CoS_6 in the experimental and optimized structures of $CoPS_3$ are grouped into two short, two medium and two long Co-S bonds. However, the sequence of the medium and long Co-S bonds is switched between the two structures. In the experimental and optimized structures of $NiPS_3$, the Ni-S bonds of NiS_6 are grouped into two short, two medium and two long Ni-S bonds. This distinction is less clear in the experimental structure. Thus, between the experimental and optimized structures of MPS_3 , the sequence of the two short, two medium and two long M-S bonds do not switch for $M = Fe$ and Ni whereas it does for $M = Co$. The latter might be the cause for why the relative stabilities of the AF1 and AF2 states in $CoPS_3$ switches between the experimental and optimized structures.

Table 2. The M-S bond distances (in Å) of the MS_6 octahedra in MPS_3 (M = Mn, Fe, Co, Ni) obtained from the experimental and the optimized crystal structures, which are shown without and with parentheses, respectively.

Mn	Fe	Co	Ni
2.627 (2.632)	2.546 (2.525)	2.485 (2.492)	2.457 (2.453)
2.627 (2.632)	2.546 (2.526)	2.485 (2.492)	2.457 (2.453)
2.625 (2.635)	2.547 (2.571)	2.504 (2.525)	2.462 (2.457)
2.625 (2.635)	2.547 (2.572)	2.504 (2.525)	2.462 (2.457)
2.634 (2.639)	2.549 (2.572)	2.491 (2.537)	2.465 (2.461)
2.634 (2.639)	2.549 (2.573)	2.491 (2.537)	2.465 (2.461)

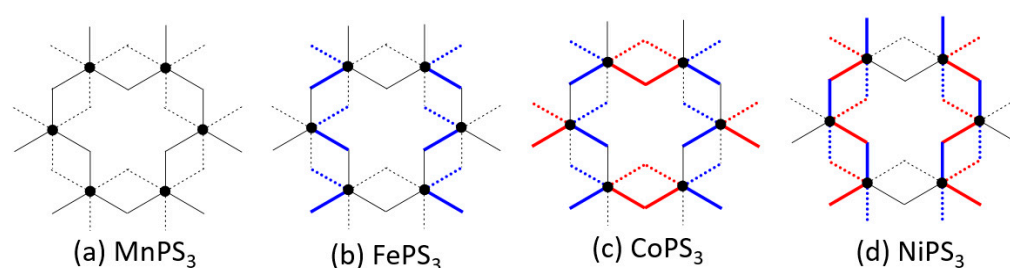


Figure 8. The arrangements of the M-S bond lengths of the MS_6 octahedra in MPS_3 . The short M-S bonds are represented by blue lines, the medium M-S bonds by red lines, and the long M-S bonds by black lines.

3.3. Preferred Spin Orientation of MPS_3

3.3.1. Quantitative Evaluation

We determine the preferred spin orientations of the M^{2+} ions in MPS_3 (M = Mn, Fe, Co, Ni) phases by performing DFT + U + SOC calculations using their FM states with the $\parallel z$ and $\perp z$ spin orientations. For the $\perp z$ direction we selected the $\parallel a$ -direction. As summarized in Table 3, these calculations predict the preferred spin orientation to be the $\parallel z$ direction for $FePS_3$, and the $\parallel x$ direction for $MnPS_3$, $CoPS_3$ and $NiPS_3$. These predictions are in agreement with experiment for $FePS_3$ [9,18], $CoPS_3$ [19], and $NiPS_3$ [20], while this is not the case for $MnPS_3$ [9,12,14,31]. Our DFT + U + SOC calculations for the AF1 state of $MnPS_3$ show that the $\parallel x$ spin orientation is still favored over the $\parallel z$ orientation just as found from the calculations using the FM state of $MnPS_3$. The Mn^{2+} spins of $MnPS_3$ were reported to have the $\parallel z$ orientation in the early studies [9,12], but were found to be slightly tilted away from the z-axis (by 8°) [14,31]. In our further discussion (see below), this small deviation is neglected.

Table 3. Relative energies (in K per formula unit) of the $\parallel z$ and $\perp z$ spin orientations of the M^{2+} ions in the FM states of MPS_3 (M = Mn, Fe, Co, Ni) obtained by DFT + U + SOC calculations. The results calculated by using the optimized (experimental) structures are presented without (with) the parentheses.

	$MnPS_3^a$	$FePS_3^b$	$CoPS_3$	$NiPS_3$
$\perp z$	0 (0)	20.0 (21.8)	0 (0)	0 (0)
$\parallel z$	0.3 (0.3)	0 (0)	3.8 (5.2)	0.8 (0.7)

^a The same result is obtained by using the AF1 state, which is the magnetic ground state of $MnPS_3$. ^b The same results are obtained from our DFT+U calculations with $U_{\text{eff}} = 3.5$ and 4.5 eV.

3.3.2. Qualitative Picture

Selection Rules of Spin Orientation and Implications

With the local z-axis of a ML_6 octahedron along its three-fold rotational axis (Figure 1a), the t_{2g} set is described by $\{1a, 1e'\}$, and the e_g set by $\{2e'\}$ [22–24], where

$$\begin{aligned} 1a &= 3z^2 - r^2 \\ \{1e'\} &= \left\{ \sqrt{\frac{2}{3}}xy - \sqrt{\frac{1}{3}}xz, \sqrt{\frac{2}{3}}(x^2 - y^2) - \sqrt{\frac{1}{3}}yz \right\} \\ \{2e'\} &= \left\{ \sqrt{\frac{1}{3}}xy + \sqrt{\frac{2}{3}}xz, \sqrt{\frac{1}{3}}(x^2 - y^2) + \sqrt{\frac{2}{3}}yz \right\} \end{aligned} \quad (5)$$

Using these d-states, the electron configurations expected for the M^{2+} ions of MPS_3 ($M = Mn, Fe, Co, Ni$) are presented in Figure 9. In the spin polarized description of a magnetic ion, the up-spin d-states lie lower in energy than the down-spin states so that the HOMO and LUMO occur in the down-spin d-states for the M^{2+} ions with more than the d^5 electron count, so only the down-spin states are shown for $FePS_3$, $CoPS_3$, and $NiPS_3$ in Figure 9a–c. For $MnPS_3$ with $d^5 Mn^{2+}$ ion, the HOMO is represented by the up-spin $1e'$, and the LUMO by the down-spin $1a$ and $2e'$ (Figure 9d).

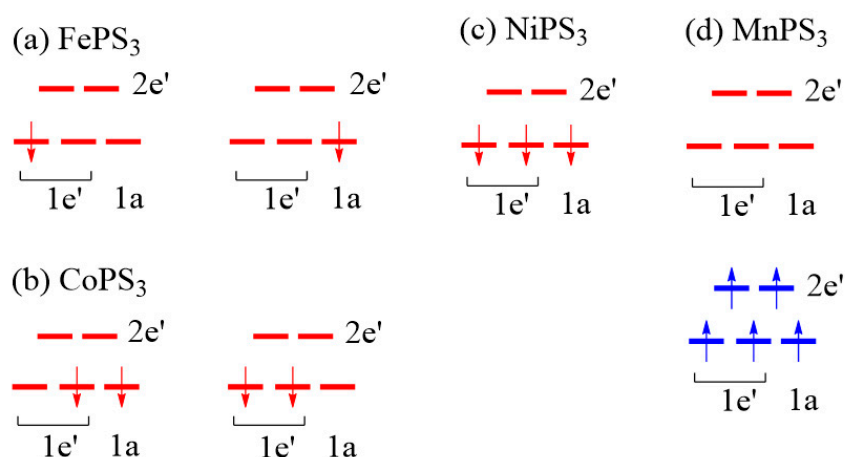


Figure 9. Electron configurations of the M^{2+} ($M = Mn, Fe, Co, Ni$) ions of (a) $FePS_3$, (b) $CoPS_3$, (c) $NiPS_3$, and (d) $MnPS_3$ in the spin polarized description. In (a–c), the up-spin d -states lying below the down-spin t_{2g} states are not shown for clarity.

In terms of the d -orbital angular states $|L, L_z\rangle$ ($L = 2, L_z = -2, -1, 0, 1, 2$), the $1e'$ state consists of the $|2, \pm 2\rangle$ and $|2, \pm 1\rangle$ sets in the weight ratio of 2:1, and the $2e'$ state in the weight ratio of 1:2 ratio. Consequently, the major component of the $1e'$ set is the $|2, \pm 2\rangle$ set, while that of the $2e'$ set is the $|2, \pm 1\rangle$ set.

The selection rules of the spin orientation are based on the $|\Delta L_z|$ value between the HOMO and LUMO of ML_n . If the HOMO and LUMO both occur in the up-spin state or in down-spin states (Figure 9a–c), the $|z$ spin orientation is predicted if $|\Delta L_z| = 0$, and the $\perp z$ spin orientation if $|\Delta L_z| = 1$. When $|\Delta L_z| > 1$, the HOMO and LUMO do not interact under SOC and hence do not affect the spin orientation. Between the $1a, 1e'$ and $2e'$ states, we note the following cases of values:

$$|\Delta L_z| = 0 \begin{cases} \text{between the major components of the } 1e' \text{ set} \\ \text{between the major components of the } 2e' \text{ set} \end{cases} \quad (6)$$

$$|\Delta L_z| = 1 \begin{cases} \text{between } 1a \text{ and the minor component of } 1e' \\ \text{between } 1a \text{ and the major component of } 2e' \\ \text{between the major components of } 1e' \text{ and } 2e' \end{cases} \quad (7)$$

We now examine the preferred spin orientations of MPS_3 from the viewpoint of the selection rules and their electron configurations (Figure 9). The d-electron configuration of FePS_3 can be either $(d\uparrow)^5(1e'\downarrow)^1$ or $(d\uparrow)^5(1a\downarrow)^1$ (Figure 9a), where the notation $(d\uparrow)^5$ indicates that all up-spin d-states are occupied. The $(d\uparrow)^5(1e'\downarrow)^1$ configuration, for which $|\Delta L_z| = 0$, predicts the $\parallel z$ spin orientation, while the $(d\uparrow)^5(1a\downarrow)^1$ configuration, for which $|\Delta L_z| = 1$, predicts the $\perp z$ spin orientation. Thus, the $(d\uparrow)^5(1a\downarrow)^1$ configuration is correct for the Fe^{2+} ion of FePS_3 . Since this configuration has the degenerate level $1e'$ unevenly occupied, it should possess uniaxial magnetism [2,3,22–24] and hence a large magnetic anisotropy energy. This is in support of the experimental finding of the Ising character of the spin lattice of FePS_3 [16] or the single-ion anisotropic character of the Fe^{2+} ion [17,18]. The d-electron configuration of CoPS_3 can be either $(d\uparrow)^5(1e'\downarrow)^2$ or $(d\uparrow)^5(1a\downarrow)^1(1e'\downarrow)^1$ (Figure 9b). The $(d\uparrow)^5(1e'\downarrow)^2$ configuration, for which $|\Delta L_z| = 1$, predicts the $\perp z$ spin orientation, while the $(d\uparrow)^5(1a\downarrow)^1(1e'\downarrow)^1$ configuration, for which $|\Delta L_z| = 0$, predicts the $\parallel z$ spin orientation. Thus, the $(d\uparrow)^5(1e'\downarrow)^2$ configuration is correct for the Co^{2+} ion of CoPS_3 . Since this configuration has the degenerate level $1e'$ evenly occupied, it does not possess uniaxial magnetism [2,3,22–24] and hence a small magnetic anisotropy energy. The d-electron configuration of NiPS_3 is given by $(d\uparrow)^5(1a)^1(1e'\downarrow)^2$ (Figure 9c), for which $|\Delta L_z| = 1$, so the $\perp z$ spin orientation is predicted in agreement with experiment.

Let us now consider the spin orientation of the Mn^{2+} ion of MnPS_3 . First, it should be noted that, if the HOMO and LUMO occur in different spin states as in MnPS_3 (Figure 9d), the selection rules predict the opposite to those found for the case when the HOMO and LUMO occur all in up-spin states or all in down-spin states [2,3,22–24]. Namely, the preferred spin orientation is the $\parallel z$ spin orientation if $|\Delta L_z| = 1$, but the $\perp z$ spin orientation if $|\Delta L_z| = 0$ [2,3,22–24]. According to Equation (7), $|\Delta L_z| = 1$ for the Mn^{2+} ion of MnPS_3 , which predicts the $\perp z$ orientation as the preferred spin direction in agreement with the quantitative estimate of the magnetic anisotropy energy obtained from the DFT + U + SOC calculations, although this is in disagreement with experiment [5,8–10]. It has been suggested that the $\parallel z$ spin orientation is caused by the magnetic dipole–dipole (MDD) interactions [13]. This subject will be probed in the following.

Magnetic Dipole–Dipole Interactions

Being of the order of 0.01 meV for two spin-1/2 ions separated by 2 Å, the MDD interaction is generally weak. For two spins located at sites i and j with the distance r_{ij} and the unit vector \mathbf{e}_{ij} along the distance, the MDD interaction is defined as [32]

$$\left(\frac{g^2 \mu_B^2}{a_0^3}\right) \left(\frac{a_0}{r_{ij}}\right)^3 \left[-3(\vec{S}_i \cdot \vec{e}_{ij})(\vec{S}_j \cdot \vec{e}_{ij}) + (\vec{S}_i \cdot \vec{S}_j) \right] \quad (8)$$

where a_0 is the Bohr radius (0.529177 Å), and $(g\mu_B)^2/a_0^3 = 0.725$ meV. The MDD effect on the preferred spin orientation of a given magnetic solid can be examined by comparing the MDD interaction energies calculated for a number of ordered spin arrangements. In summing the MDD interactions between various pairs of spin sites, it is necessary to employ the Ewald summation method [33–35]. Table 4 summarizes the MDD interaction energies calculated, by using the optimized structures of MPS_3 ($M = \text{Mn, Fe, Co, Ni}$), for the $\parallel z$ and $\parallel x$ spin directions in the AF1, AF2 and AF3 states. The corresponding results obtained by using the experimental structures of MPS_3 are summarized in Table S1.

Table 4. Relative energies (in K per formula unit) of the $\parallel x$ and $\parallel z$ spin orientations calculated by MDD calculations for the M^{2+} ions of MPS_3 ($M = Mn, Fe, Co, Ni$) in the AF1, AF2 and AF3 states using the optimized crystal structures.

	$MnPS_3$		$FePS_3$		$CoPS_3$		$NiPS_3$	
	$\parallel x$	$\parallel z$	$\parallel x$	$\parallel z$	$\parallel x$	$\parallel z$	$\parallel x$	$\parallel z$
AF1	0.48	0.17	0.36	0.12	0.21	0.07	0.09	0.03
AF2	0.00	0.35	0.00	0.26	0.00	0.15	0.00	0.07
AF3	0.55	0.38	0.38	0.27	0.22	0.15	0.10	0.07

These results can be summarized as follows: for the $\parallel z$ spin orientation, the AF1 state is more stable than the AF2 and AF3 states. For the $\parallel x$ spin orientation, the AF2 state is more stable than the AF1 and AF3 states. The $\parallel x$ spin direction of the AF2 state is more stable than the $\parallel z$ spin direction of the AF1 state. However, none of these results can reverse the relative stabilities of the $\parallel z$ and $\parallel x$ spin directions determined for $FePS_3$, $CoPS_3$, and $NiPS_3$ from the DFT + U + SOC calculations (Table 3). The situation is slightly different for $MnPS_3$, which adopts the AF1 state as the magnetic ground state. For $MnPS_3$ in this state, the MDD calculations predict that the $\parallel z$ spin orientation is more stable than the $\parallel x$ spin orientation by 0.3 K per formula unit (Table 4). Note that this prediction is the exact opposite to what the DFT + U + SOC calculations predict for $MnPS_3$ in the AF1 state (Table 3). Thus, the balance between these two opposing energy contributions will determine whether the $\parallel z$ spin orientation is more stable than the $\perp z$ spin orientation in agreement with the experimental observation. Consequently, for $MnPS_3$ the MDD interaction dominates over the SOC effect which is plausible because of the half-filled shell electronic configuration. This is because the AF1 magnetic structure is forced on $MnPS_3$; in terms of purely MDD interactions alone, the $\perp z$ spin orientation in the AF2 state is most stable.

3.4. Quantitative Evaluations of Spin Exchanges

Due to the monoclinic crystal structure that MPS_3 adopts, each of the exchanges J_{12} , J_{13} and J_{14} (Figure 10a) are expected to split into two slightly different spin exchanges (Figure 10b) so that there are six spin exchanges J_1 – J_6 to consider. To extract the values of the six spin exchanges J_1 – J_6 (Figure 3), we employ the spin Hamiltonian expressed as:

$$H_{\text{spin}} = - \sum_{i>j} J_{ij} \hat{S}_i \cdot \hat{S}_j \quad (9)$$

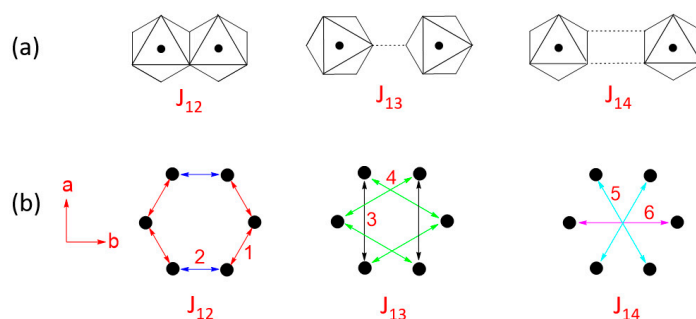


Figure 10. (a) Three kinds of spin exchange paths in each honeycomb layer of MPS_3 . (b) Two kinds of the spin exchanges resulting from J_{12} , J_{13} and J_{14} due to the loss of the trigonal symmetry in the MPS_3 honeycomb layers. In (b), the numbers 1–6 refer to J_1 – J_6 , respectively.

Then, the energies of the FM and AF1–AF6 states of MPS_3 ($M = Mn, Fe, Co, Ni$) per $2 \times 2 \times 1$ supercell are written as:

$$\begin{aligned} E_{FM} &= (-16J_1 - 8J_2 - 16J_3 - 32J_4 - 16J_5 - 8J_6)S^2 \\ E_{AF1} &= (+16J_1 + 8J_2 - 16J_3 - 32J_4 + 16J_5 + 8J_6)S^2 \\ E_{AF2} &= (-16J_1 + 8J_2 - 16J_3 + 32J_4 + 16J_5 + 8J_6)S^2 \\ E_{AF3} &= (-8J_2 + 16J_3 + 16J_5 + 8J_6)S^2 \\ E_{AF4} &= (+16J_1 - 8J_2 - 16J_3 + 32J_4 - 16J_5 - 8J_6)S^2 \\ E_{AF5} &= (+8J_2 + 16J_3 - 16J_5 + 8J_6)S^2 \\ E_{AF6} &= (-8J_2 + 16J_3 + 16J_5 - 8J_6)S^2 \end{aligned}$$

where S is the spin on each M^{2+} ion (i.e., $S = 5/2, 2, 3/2$ and 1 for $M = Mn, Fe, Co$, and Ni , respectively). By mapping the relative energies of the FM and AF1–AF6 states determined in terms of the spin exchange J_1 – J_6 onto the corresponding relative energies obtained from the DFT + U calculations (Table 1), we find the values of J_1 – J_6 listed in Table 5. (The spin exchanges of MPS_3 determined by using their experimental crystal structures are summarized in Table S2)

Table 5. Spin exchanges J_1 – J_6 obtained (for the optimized structures of MPS_3 ($M = Mn, Fe, Co, Ni$) from DFT + U calculations with $U_{eff} = 4$ eV) by simulating the relative energies of the FM and AF1–AF6 states with the six spin exchanges.

	Mn	Fe	Co	Ni
J_1	1.00	0.37	0.05	−0.25
J_2	0.87	−0.32	−0.91	−0.14
J_3	0.06	0.36	−0.55	0.04
J_4	0.05	0.07	0.04	−0.01
J_5	0.34	0.86	0.11	0.99
J_6	0.33	1.00	1.00	1.00
	$J_1 = -16.0$ K	$J_6 = -18.4$ K	$J_6 = -608.7$ K	$J_6 = -172.4$ K

With the sign convention adopted in Eq. 1, AFM exchanges are represented by $J_{ij} < 0$, and FM exchanges by $J_{ij} > 0$. From Table 5, the following can be observed:

- In all MPS_3 ($M = Mn, Fe, Co, Ni$), $J_1 \neq J_2$, $J_3 \neq J_4$, and $J_5 \neq J_6$, reflecting that the exchange paths are different between J_1 and J_2 , between J_3 and J_4 , and between J_5 and J_6 (Figure 10).
- $J_1 \approx J_2 < 0$, $J_3 \approx J_4 \approx 0$, and $J_5 \approx J_6 < 0$ for $MnPS_3$ while $J_1 \approx J_2 > 0$, $J_3 \approx J_4 \approx 0$, and $J_5 \approx J_6 < 0$ for $NiPS_3$. To a first approximation, the electron configurations of $MnPS_3$ and $NiPS_3$ can be described by $(t_{2g})^3(e_g)^2$ and $(t_{2g})^6(e_g)^2$, respectively. That is, they do not possess an unevenly occupied degenerate state t_{2g} .
- In $FePS_3$ and $CoPS_3$, J_1 and J_2 are quite different, and so are J_3 and J_4 . While J_5 and J_6 are comparable in $FePS_3$, they are quite different in $CoPS_3$. The electron configurations of $FePS_3$ and $NiPS_3$ can be approximated by $(t_{2g})^4(e_g)^2$ and $(t_{2g})^5(e_g)^2$, respectively. Namely, they possess an unevenly occupied degenerate state t_{2g} .
- The strongest exchange is J_1 in $MnPS_3$, but J_6 in other MPS_3 ($M = Fe, Co, Ni$).
- The second NN exchange J_3 is strongly FM in $CoPS_3$, while the third NN exchange J_6 is very strongly AFM in $CoPS_3$ and $NiPS_3$.

From the viewpoints of the expected trends in spin exchanges, the observation (e) is quite unusual. This will be discussed in the next section.

3.5. Unusual Features of the M-L ... L-M Spin Exchanges

3.5.1. Second Nearest-Neighbor Exchange

As pointed out in the previous section, the second NN exchange J_3 of CoPS_3 is strongly FM despite that it is a M-L ... L-M exchange to a first approximation. This implies that the J_F component in some (φ_i, φ_j) exchanges is nonzero, namely, the overlap electron density associated with those exchanges is nonzero. This implies that the p-orbital tails of the two magnetic orbitals are hybridized with the group orbitals of the $\text{P}_2\text{S}_6^{4-}$ anion, i.e., they become delocalized into the whole $\text{P}_2\text{S}_6^{4-}$ anion. Each MS_6 octahedron has three mutually orthogonal “ MS_4 square planes” containing the yz , xz and xy states (Figure 11a). At the four corners of these three square planes, the p-orbital tails of the d-states are present (Figure 3a).

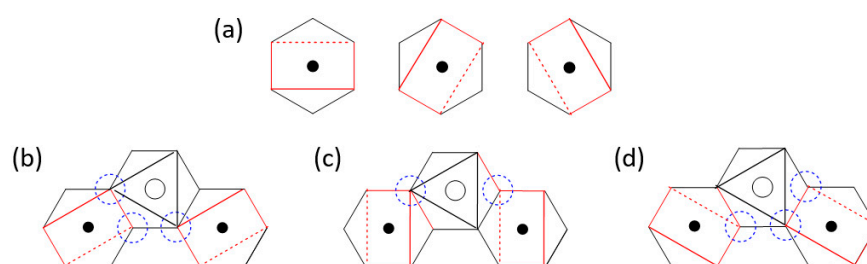


Figure 11. (a) Three MS_4 square planes of a MS_6 octahedron, containing the xy , xz and yz states of an MS_6 octahedron. (b–d) Three cases of the CoS_4 square planes containing the t_{2g} magnetic orbitals in the J_3 exchange path of CoPS_3 .

The lone-pair orbitals of the S atoms are important for the formation of each MS_6 octahedron. Due to the bonding requirement of the $\text{P}_2\text{S}_6^{4-}$ anion, such lone pair orbitals become symmetry-adapted. An example in which the p-orbitals of all the S atoms are present is shown in Figure 1e.

With the $(t_{2g})^5(e_g)^2$ configuration, the Co^{2+} ion of CoPS_3 has five electrons in the t_{2g} level, namely, it has only one t_{2g} magnetic orbital. This magnetic orbital is contained in one of the three CoS_4 square planes presented in Figure 11b–d. When the S p-orbital at one corner of the $\text{P}_2\text{S}_6^{4-}$ anion interacts with a d-orbital of M, the S p-orbitals at the remaining corners are also mixed in. Thus, when $\text{P}_2\text{S}_6^{4-}$ anion shares corners with both MS_4 square planes of the J_3 exchange path, a nonzero overlap electron density is generated, thereby making the spin exchange FM. For convenience, we assume that the magnetic t_{2g} orbital of the Co^{2+} ion is the xy state. Then, there will be not only the (xy, xy) exchange, but also the $(xy, x^2 - y^2)$ and $(x^2 - y^2, xy)$ exchanges between the two Co^{2+} ions of the J_3 path. All these individual exchanges lead to nonzero overlap electron densities by the delocalization of the p-orbital tails with the group orbitals of the molecular anion $\text{P}_2\text{S}_6^{4-}$. In other words, the spin exchange J_3 in CoPS_3 is nominally a M-L ... L-M, which is expected to be AFM by the qualitative rule, but it is strongly FM. It is clear that, if the L ... L linkage is a part of the covalent framework of a molecular anion such as $\text{P}_2\text{S}_6^{4-}$, a nominal M-L ... L-M exchange can become FM for a certain combination of the d-electron count of the metal M and the geometries of the exchange path.

3.5.2. Third Nearest-Neighbor Exchange

Unlike in MnPS_3 and FePS_3 , the M-S ... S-M exchange J_6 is unusually strong in CoPS_3 and NiPS_3 (Section 3.3). This is so despite that the S ... S contact distances are longer in CoPS_3 and NiPS_3 than in MnPS_3 and FePS_3 (i.e., the S ... S contact distance of the J_6 path in MPS_3 is 3.409, 3.416, 3.421 and 3.450 Å for M = Mn, Fe, Co and Ni, respectively). We note that a strong M-L ... L-M exchange (i.e., a spin exchange leading to a large energy split Δe_{ij}) becomes weak, when the L ... L contact is bridged by a d^0 cation like, e. g., V^{5+} and W^{6+} to form the M-L ... A ... L-M exchange path (Figure 6b), because the out-of-phase combination ψ_- is lowered in energy by interacting with the unoccupied d_π orbital of the cation A. Conversely, then, one may ask if the

strength of a M-L ... L-M spin exchange can be enhanced by raising the ψ_- level. The latter can be achieved if the L ... L path provides an occupied level of π -symmetry that can interact with ψ_- . As depicted in Figure 12a, the J_6 path has the two MS_4 square planes containing the x^2-y^2 magnetic orbitals (Figure 12b). The lone-pair group orbital of the S_4 rectangular plane (Figure 12c) of the $P_2S_6^{4-}$ anion has the correct symmetry to interact with ψ_- , so that the ψ_- level is raised in energy thereby enlarging the energy split between ψ_+ and ψ_- and strengthening the J_6 exchange (Figure 12d). Although this reasoning applies equally to $MnPS_3$ and $FePS_3$, the latter do not have a strong J_6 exchange. This can be understood by considering Equation (1), which shows that a magnetic ion with several magnetic orbitals leads to several individual spin exchanges that can lead to FM contributions.

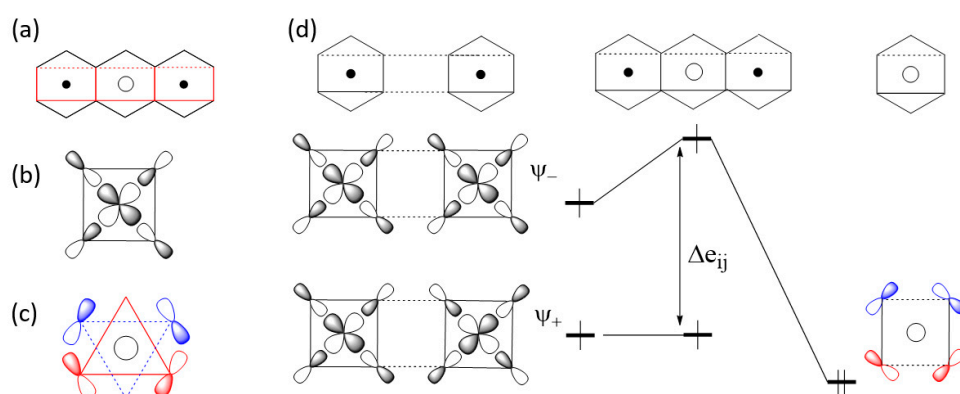


Figure 12. (a) The J_6 spin exchange path of MPS_3 ($M = Co, Ni$) viewed in terms of the MS_4 and P_2S_4 square planes. (b) The x^2-y^2 magnetic orbital of the MS_6 octahedron. (c) The S p-orbitals present at the corners of the P_2S_4 square plane. (d) How the M-S ... S-M spin exchange is enhanced by the through-bond effect of the intervening P_2S_6 octahedron.

In view of the above discussion, which highlights the unusual nature of the second and third NN spin exchanges mediated by a molecular anion such as $P_2S_6^{4-}$, we propose to use the notation M-(L-L)-M to distinguish it from M-L-M. M-L ... L-M and M-L ... A ... L-M type exchanges. The notation (L-L) indicates two different ligand sites of a multidentate molecular anion, each with lone pairs for the coordination with a cation M. Such M-(L-L)-M exchanges can be strongly FM or strongly AFM, as discussed above. Currently, there are no qualitative rules with which to predict whether they will be FM or AFM. A similar situation was found, for example, for the mineral Azurite $Cu_3(CO_3)_2(OH)_2$, in which every molecular anion CO_3^{2-} participates in three different Cu-(O-O)-Cu exchanges. DFT + U calculations show that one of these three is substantially AFM, but the remaining two are negligible. So far, this observation has not been understood in terms of qualitative reasoning.

3.6. Description Using Three Exchanges

Experimentally, the magnetic properties of MPS_3 have been interpreted in terms of three exchange parameters, namely, by assuming that $J_1 = J_2$ ($\equiv J_{12}$), $J_3 = J_4$ ($\equiv J_{13}$), and $J_5 = J_6$ ($\equiv J_{14}$). To investigate whether this simplified description is justified, we simulate the relative energies of the seven ordered spin states of MPS_3 by using the three exchanges J_{12} , J_{13} and J_{14} as parameters in terms of the least-square fitting analysis. Our results, summarized in Table 6, show that the standard deviations of J_{12} , J_{13} and J_{14} are small for $MnPS_3$ and $NiPS_3$, moderate in $FePS_3$, but extremely large in $CoPS_3$ (for details, see Figures S2–S5). The exchanges experimentally deduced for $FePS_3$ are $J_{12} = -17$ K, $J_{13} = -0.5$ K, and $J_{14} = 7$ K from neutron inelastic scattering measurements [17], -17 K $\leq J_{12} \leq -5.6$ K, -7.2 K $\leq J_{13} \leq 2.8$ K, and $0 \leq J_{14} \leq 10$ K from powder susceptibility measurements [9], and $J_{12} = -19.6$ K, $J_{13} = 10.3$ K, and $J_{14} = -2.2$ K from high field measurements [17]. These experimental estimates are dominated by J_{12} , but the theoretical

estimates of Table 6 by J_{14} . One might note from Table 6 that the magnetic properties of MnPS_3 , FePS_3 and NiPS_3 can be reasonably well approximated by two exchanges, that is, by J_{12} and J_{14} for MnPS_3 , by J_{14} and J_{12} for NiPS_3 , and by J_{14} and J_{13} for FePS_3 . However, this three-parameter description leads to erroneous predictions for the magnetic ground states of MPS_3 ; it predicts the AF1 state to be the ground state for both MnPS_3 and CoPS_3 . This prediction is correct for MnPS_3 , but incorrect for CoPS_3 . In addition, it predicts that the AF2 and AF3 states possess the same stability for all MPS_3 ($M = \text{Mn, Fe, Co, Ni}$), and are the ground states for FePS_3 and NiPS_3 . These two predictions are both incorrect.

Table 6. Spin exchanges J_{12} , J_{13} and J_{14} in K obtained (for the optimized structures of MPS_3 ($M = \text{Mn, Fe, Co, Ni}$) from DFT + U calculations with $U_{\text{eff}} = 4$ eV) by simulating the relative energies of the FM and AF1–AF6 states with the three spin exchanges.

	Mn	Fe	Co	Ni
J_{12}	-15.5 ± 0.4	2.0 ± 7.7	-61.4 ± 119.0	36.3 ± 4.3
J_{13}	-0.9 ± 0.2	-7.7 ± 3.9	60.7 ± 55.3	0.0 ± 2.0
J_{14}	-5.3 ± 0.3	-20.9 ± 4.5	-59.1 ± 95.6	-186.0 ± 3.4

4. Concluding Remarks

Our DFT + U calculations for the optimized structures of MPS_3 ($M = \text{Mn, Fe, Co, Ni}$) reveal that, in agreement with experiment, the magnetic ground state of MnPS_3 is the AF1 state while those of CoPS_3 and NiPS_3 are the AF2 state. In disagreement with experiment, however, our calculations predict the AF2 state to be the magnetic ground state for FePS_3 . Our DFT + U + SOC calculations show that, in agreement with experiment, the preferred spin orientation of FePS_3 is the $\parallel z$ direction while those of CoPS_3 and NiPS_3 are the $\perp z$ direction, and the Fe^{2+} ion of FePS_3 exhibits uniaxial anisotropy. In disagreement with experiment, these calculations predict the preferred spin orientation for MnPS_3 to be the $\perp z$ direction. Our analyses suggest that the $\parallel z$ spin direction experimentally observed for the Mn^{2+} ions arises from the magnetic dipole–dipole interactions in the AF1 magnetic state. We presented simple qualitative rules governing spin exchanges to be used as guidelines for gauging the nature of various spin exchanges. These rules allowed us to recognize several unusual exchanges of MPS_3 ; the second NN exchange J_3 of CoPS_3 is strongly FM while the third NN exchanges J_6 of CoPS_3 and NiPS_3 are very strongly AFM. These observations reflect the fact that the lone-pair orbitals of the $\text{P}_2\text{S}_6^{4-}$ ion, mediating the spin exchanges in MPS_3 are symmetry-adapted group orbitals, so the effect of coordinating one S atom to one M^{2+} ion is felt by all the remaining five S atoms of $\text{P}_2\text{S}_6^{4-}$. The spin exchanges mediated by molecular anions, termed the M-(L-L)-M type exchanges, differ in nature from the M-L-M, M-L ... L-M and M-L ... A ... L-M type exchanges. To find qualitative trends in the M-(L-L)-M type exchanges, it is necessary to further study the spin exchanges involving various other molecular anions.

Supplementary Materials: The following are available online. Figure S1: Ordered spin states, FM, AF4, AF5 and AF6 employed together with the states AF1, AF2 and AF3 (see the text) to determine the magnetic ground states as well as the spin exchanges J_1 – J_6 of MPS_3 ($M = \text{Mn, Fe, Co, Ni}$). Figure S2–S5. Results of the least-square fitting the relative energies of the seven ordered spin states (FM, AF1–AF6) of MnPS_3 , CoPS_3 and FePS_3 , and NiPS_3 , Table S1: Relative energies (in K per formula unit) of the $\parallel x$ and $\parallel z$ spin orientations obtained by MDD calculations for the M^{2+} ions of MPS_3 ($M = \text{Mn, Fe, Co, Ni}$) in the AFM1, AF2 and AFM3 states using the experimental crystal structures. Table S2: Spin exchanges (in K) obtained for the experimental structures of MPS_3 ($M = \text{Mn, Fe, Co, Ni}$) from DFT + U calculations with $U_{\text{eff}} = 4$ eV.

Author Contributions: Conceptualization, M.-H.W.; formal analysis and investigation, H.-J.K., R.K. and M.-H.W.; resources, H.-J.K.; data curation, H.-J.K.; writing—original draft preparation, M.-H.W.; writing—review and editing, H.-J.K., R.K. and M.-H.W.; visualization, M.-H.W.; supervision, M.-

H.W.; funding acquisition, H.-J.K. All authors have read and agreed to the published version of the manuscript.

Funding: The work at Kyung Hee University was supported by the Basic Science Research Program through the National Research Foundation of Korea (NRFK) funded by the Ministry of Education (2020R1A6A1A03048004).

Institutional Review Board Statement: Not applicable.

Informed Consent Statement: Not applicable.

Acknowledgments: H.-J. K. thanks the NRFK for the fund 2020R1A6A1A03048004.

Conflicts of Interest: The authors declare no conflict of interest.

References

1. Whangbo, M.-H.; Koo, H.-J.; Dai, D. Spin exchange interactions and magnetic structures of extended magnetic solids with localized spins: Theoretical descriptions on formal, quantitative and qualitative levels. *J. Solid State Chem.* **2003**, *176*, 417–481. [[CrossRef](#)]
2. Xiang, H.J.; Lee, C.; Koo, H.-J.; Gong, X.; Whangbo, M.-H. Magnetic properties and energy-mapping analysis. *Dalton Trans.* **2013**, *42*, 823–853. [[CrossRef](#)]
3. Whangbo, M.-H.; Xiang, H.J. Magnetic Properties from the Perspectives of Electronic Hamiltonian: Spin Exchange Parameters, Spin Orientation and Spin-Half Misconception. In *Handbook in Solid State Chemistry, Volume 5: Theoretical Descriptions*; Wiley: New York, NY, USA, 2017; pp. 285–343.
4. Whangbo, M.-H.; Koo, H.-J.; Kremer, R.K. Spin Exchanges Between Transition-Metal Ions Governed by the Ligand p-Orbitals in Their Magnetic Orbitals. *Molecules* **2021**, *26*, 531. [[CrossRef](#)]
5. Goodenough, J.B.; Loeb, A.L. Theory of ionic ordering, crystal distortion, and magnetic exchange due to covalent forces in spinels. *Phys. Rev.* **1955**, *98*, 391–408. [[CrossRef](#)]
6. Goodenough, J.B. Theory of the role of covalence in the perovskite-type manganites [La, M(II)]MnO₃. *Phys. Rev.* **1955**, *100*, 564–573. [[CrossRef](#)]
7. Kanamori, J. Superexchange interaction and symmetry properties of electron orbitals. *J. Phys. Chem. Solids* **1959**, *10*, 87–98. [[CrossRef](#)]
8. Goodenough, J.B. *Magnetism and the Chemical Bond*; Interscience; Wiley: New York, NY, USA, 1963.
9. Kurosawa, K.; Saito, S.; Yamaguchi, Y. Neutron diffraction study on MnPS₃ and FePS₃. *J. Phys. Soc. Jpn.* **1983**, *52*, 3919–3926. [[CrossRef](#)]
10. Ouvrard, G.; Brec, R.; and Rouxel, J. Structural determination of some MPS₃ phases (M = Mn, Fe, Co, Ni and Cd). *Mater. Res. Bull.* **1985**, *20*, 1181–1189. [[CrossRef](#)]
11. Brec, R. Review on structural and chemical properties of transition metal phosphorus trisulfides MPS₃. *Solid State Ionics* **1986**, *22*, 3–30. [[CrossRef](#)]
12. Kuroda, K.; Kurosawa, K.; Shozo, S.; Honda, M.; Zhihong, Y.; Date, M. Magnetic-properties of layered compound MnPS₃. *J. Phys. Soc. Jpn.* **1986**, *55*, 4456–4463.
13. Hicks, T.J.; Keller, T.; Wildes, A.R. Magnetic dipole splitting of magnon bands in a two-dimensional antiferromagnet. *J. Magn. Magn. Mater.* **2019**, *474*, 512–516. [[CrossRef](#)]
14. Ressouche, E.; Loire, M.; Simonet, V.; Ballou, L.; Stunault, A.; Wildes, A. Magnetoelectric MnPS₃ as a candidate for ferrotoroidicity. *Phys. Rev. B* **2010**, *82*, 100408(R). [[CrossRef](#)]
15. Okuda, K.; Kurosawa, K.; Saito, S. High field magnetization process in FePS₃. In *High Field Magnetism*; Date, M., Ed.; Elsevier: North Holland, Amsterdam, The Netherlands, 1983; pp. 55–58.
16. Rule, K.C.; McIntyre, G.J.; Kennedy, S.J.; Hicks, T.J. Single-crystal and powder neutron diffraction experiments on FePS₃: Search for the magnetic structure. *Phys. Rev. B* **2007**, *76*, 134402. [[CrossRef](#)]
17. Wildes, A.R.; Rule, K.C.; Bewley, R.I.; Enderle, M.; Hicks, T.J. The magnon dynamics and spin exchange parameters of FePS₃. *J. Phys. Condens. Matter* **2012**, *24*, 416004. [[CrossRef](#)]
18. Lançon, D.; Walker, H.C.; Ressouche, E.; Ouladiaf, B.; Rule, K.C.; McIntyre, G.J.; Hicks, T.J.; Rønnow, H.M.; Wildes, A.R. Magnetic structure and magnon dynamics of the quasi-two-dimensional antiferromagnet FePS₃. *Phys. Rev. B* **2016**, *94*, 214407. [[CrossRef](#)]
19. Wildes, A.R.; Simonet, V.; Ressouche, E.; Ballou, R.; McIntyre, G.J. The magnetic properties and structure of the quasi-two-dimensional antiferromagnet CoPS₃. *J. Phys. Condens. Matter* **2017**, *29*, 455801. [[CrossRef](#)]
20. Wildes, A.R.; Simonet, V.; Ressouche, E.; McIntyre, G.J.; Avdeev, M.; Suard, E.; Kimber, S.A.J.; Lançon, D.; Pepe, G.; Moubaraki, B.; et al. Magnetic structure of the quasi-two-dimensional antiferromagnet NiPS₃. *Phys. Rev. B* **2015**, *92*, 224408. [[CrossRef](#)]
21. Chittari, B.L.; Park, Y.J.; Lee, D.K.; Han, M.S.; MacDonal, A.H.; Hwang, E.H.; Jung, J.I. Electronic and magnetic properties of single-layer MPX₃ metal phosphorous trichalcogenides. *Phys. Rev. B* **2016**, *94*, 184428. [[CrossRef](#)]
22. Whangbo, M.-H.; Gordon, E.E.; Xiang, H.J.; Koo, H.-J.; Lee, C. Prediction of spin orientations in terms of HOMO-LUMO interactions using spin-orbit coupling as perturbation. *Acc. Chem. Res.* **2015**, *48*, 3080–3087. [[CrossRef](#)]

23. Gordon, E.E.; Xiang, H.J.; Köhler, J.; Whangbo, M.-H. Spin orientations of the spin-half Ir^{4+} ions in $\text{Sr}_3\text{NiIrO}_6$, Sr_2IrO_4 and Na_2IrO_3 : Density functional, perturbation theory and Madelung potential analyses. *J. Chem. Phys.* **2016**, *144*, 114706. [[CrossRef](#)]
24. Whangbo, M.-H.; Xiang, H.J.; Koo, H.-J.; Gordon, E.E.; Whitten, J.L. Electronic and Structural Factors Controlling the Spin Orientations of Magnetic Ions. *Inorg. Chem.* **2019**, *58*, 11854–11874. [[CrossRef](#)]
25. Hay, P.J.; Thibault, J.C.; Hoffmann, R. Orbital interactions in metal dimer complexes. *J. Am. Chem. Soc.* **1975**, *97*, 4884–4899. [[CrossRef](#)]
26. Kresse, G.; Furthmüller, J. Efficiency of ab-initio total energy calculations for metals and semiconductors using a plane-wave basis set. *Comput. Mater. Sci.* **1996**, *6*, 15–50. [[CrossRef](#)]
27. Kresse, G.; Joubert, D. From ultrasoft pseudopotentials to the projector augmented-wave method. *Phys. Rev. B* **1999**, *59*, 1758–1775. [[CrossRef](#)]
28. Perdew, J.P.; Burke, K.; Ernzerhof, M. Generalized Gradient Approximation Made Simple. *Phys. Rev. Lett.* **1996**, *77*, 3865. [[CrossRef](#)]
29. Dudarev, S.L.; Botton, G.A.; Savrasov, S.Y.; Humphreys, C.J.; Sutton, A.P. Electron-energy-loss spectra and the structural stability of nickel oxide: An LSDA+U study. *Phys. Rev. B* **1998**, *57*, 1505. [[CrossRef](#)]
30. Kuneš, K.; Novák, P.; Schmid, R.; Blaha, P.; Schwarz, K. Electronic structure of fcc Th: Spin-orbit calculation with $6p_{1/2}$ local orbital extension. *Phys. Rev. Lett.* **2001**, *64*, 153102.
31. Vaclavkova, D.; Delhomme, A.; Faugeras, C.; Potemski, M.; Bogucki, A.; Suffczyński, J.; Kossacki, P.; Wildes, A.R.; Grémaud, B.; Saúl, A. Magnetoelastic interaction in the two-dimensional magnetic material MnPS_3 studied by first principles calculations and Raman experiments. *2D Mater.* **2020**, *7*, 035030. [[CrossRef](#)]
32. Koo, H.-J.; Xiang, H.J.; Lee, C.; Whangbo, M.-H. Effect of Magnetic Dipole-Dipole Interactions on the Spin Orientation and Magnetic Ordering of the Spin-Ladder Compound $\text{Sr}_3\text{Fe}_2\text{O}_5$. *Inorg. Chem.* **2009**, *48*, 9051. [[CrossRef](#)]
33. Ewald, P.P. Die Berechnung Optischer und Elektrostatischer Gitterpotentiale. *Ann. Phys.* **1921**, *64*, 253. [[CrossRef](#)]
34. Darden, T.; York, D.; Pedersen, L. Particle mesh Ewald: An $N \cdot \log(N)$ method for Ewald sums in large systems. *J. Chem. Phys.* **1993**, *98*, 10089. [[CrossRef](#)]
35. Wang, H.; Dommert, F.; Holm, C. Optimizing working parameters of the smooth particle mesh Ewald algorithm in terms of accuracy and efficiency. *J. Chem. Phys.* **2010**, *133*, 034117. [[CrossRef](#)] [[PubMed](#)]